GAZE-DRIVEN APPROACH FOR ESTIMATING LUMINANCE VALUES IN THE FIELD OF VIEW FOR DISCOMFORT GLARE ASSESSMENTS

Sarey Khanie M. [1], Stoll J.[2], Einhäuser W. [2], Wienold J.[1], Andersen M.[1]
[1] Interdisciplinary Laboratory of Performance Integrated Design (LIPID), EPFL, Lausanne, SWITZERLAND, [2] Neurophysics Department, Philipps-Universität, Marburg, GERMANY
mandana.sareykhanie@epfl.ch

Abstract

A gaze-driven methodology for discomfort glare was developed and applied for glare evaluation. A series of user assessments were performed in an office-like test laboratory under various lighting conditions. The participants' gaze responses were recorded by means of mobile eye tracking while monitoring photometric quantities relevant to visual comfort using HDR luminance imaging. The integration of the luminance images coupled with eye-tracking methods enabled us to use gaze-centred luminance distribution to have an accurate estimate of the light received at the eye. Using a novel gaze-driven approach, a unique database was created as a basis to investigate the gaze direction dependencies of visual comfort. Here we compare the proposed gaze-driven approach with two other approaches based on fixed-gaze assumptions: gaze fixating on the task area, and gaze shifted 45 ° towards the window area. The results show that there is a significant difference between luminance distributions driven by gaze and those based on fixed-gaze assumptions, indicating a potentially important impact on glare assessment results as well.

Keywords: Discomfort glare, HDR imaging techniques, Eye-tracking methods, Gaze Direction

1 Introduction

Predicting visual comfort in indoor environments still poses challenges when determining a lighting or daylighting scheme. Ensuring visually comfortable lighting solutions in indoor environments currently revolves mainly around minimising the periods of visual discomfort caused by light. One of the main causes of visual discomfort is known as discomfort glare. This type of glare is a distracting or uncomfortable situation, which interferes with the perception of visual information but does not significantly reduce the ability to see the information needed for visual activities (CIE 1983). The quantification attempts made on discomfort glare are based on subjective assessments and have led to the development of a series of different metrics. Among the more commonly known discomfort glare metrics daylight glare index (DGI) (Hopkinson 1972) and daylight glare probability (DGP) have been developed specifically for daylight situations (Wienold & Christoffersen 2006).

The developed metrics are very similar to one another, as they share the same basic form for a specific FOV (Boyce, 2014). This form accounts for four main physical quantities in relation to subjective judgment of the sensation of discomfort as expressed in equation (1). The four physical quantities are the luminance of the glare source (L_s) the solid angle of the glare source subtended at the eye (ω_s), the discomfort sensation the glare source induces based on its angular position in the FOV with respect to the gaze direction (P_i) and the adaptation luminance (L_a) and (exp_i) is a model-specific parameter equation.

$$G \approx \sum \frac{L_s^{exp_1} \omega_s^{exp_2}}{L_a^{exp_3} P^{exp_4}} \quad (1)$$

One of the major limitations shared by these and other discomfort glare metrics is that they do not integrate the dependencies of visual perception on the dynamic shifts of gaze: the assumption made by these metrics is that the gaze direction is fixed. Changes in gaze direction will, however, have a strong impact on the assumed position of the disturbing glare source in the field of view (FOV) (Luckiesh & Guth 1949, Kim et al. 2009, Clear 2012). Shifts of gaze can result in changes of overall light levels entering the eye, requiring the visual system to adapt its sensitivity to light (Kokoschka & Haubner 1985). The changes in gaze direction thus have indirect implications on adaptation levels and consequently, on the

subjective response to glare sensation. Thus, the dynamics of gaze direction may exert significant impact on glare evaluation outcomes.

Gaze allocations are typically studied in terms of fixations (periods of pause) and saccades (rapid movements between fixations) with respect to temporal and spatial characteristics, e.g. duration or dispersion (Salvucci 2000). So-called *saccades* constitute a prominent class of eye movements in humans; saccades are extremely rapid (up to about 500°/s) shifts in eye position that occur about 3 times each second. Other types of eye movement include smooth pursuit to follow isolated moving objects, the vestibular ocular reflex (VOR) to stabilise gaze during self-motion, the optokinetic nystagmus (OKN) to stabilise gaze during movement of the scene, vergence movements to allocate gaze in depth as well as several classes of tiny movements (drift, micro-saccades and tremor) that occur while the eye is fixating.

It is generally agreed upon that visual and cognitive processing occurs during fixations, when the retinal image from the visual environment is stabilised. Very few studies so far have investigated the relationship between gaze shifts and building-induced visual context, such as the presence of window (Sury et al. 2010, Hubalek & Schierz 2004) or light (Kokoschka & Haubner 1985, Jakubiec & Reinhart 2012, Vincent et al. 2009, Nuthmann & Einhäuser 2015). These studies suggest that gaze directions extend over different regions of the space on vertical and horizontal planes and thus are not solely fixed on a certain area (Hubalek & Schierz 2004) . In other studies the necessity of limited luminance ratios at workplaces have been underlined for minimising performance losses due to re-adaptation process caused by dynamics of gaze direction (Kokoschka & Haubner 1985). The adaptive capability of gaze shifts in response to uncomfortable conditions was also acknowledged by (somewhat arbitrarily) extending gaze directions to a predefined angular range rather than to a unique gaze direction (Jakubiec & Reinhart 2012). Recent eye-tracking studies with static images of natural scenes have in turn shown a tendency of observers to avoid bright and dark stimulus regions and to direct gaze to regions of medium luminance (Vincent et al. 2009, Nuthmann & Einhäuser 2015). To our knowledge, no study has gone as far as to relate the actual gaze direction to light-induced discomfort perception in indoor environments.

2 Methodology

To study the relations between gaze patterns and visual discomfort, we employed mobile eye-tracking methods in our discomfort glare assessment experimental study in addition to the commonly used subjective assessment methods which we will summarize below. Resorting to eye-tracking methods is a novel approach in discomfort glare assessments that allows for gaze-driven luminance field estimation as opposed to fixed gaze luminance field. Gaze-driven luminance distribution gives us an estimation of luminance values actually perceived by the participants.

2.1 Office setup

The experiments were performed from July to mid-October in an experimental facility specifically designed for this type of studies at the Fraunhofer Institute for Solar Energy Systems (ISE) in Freiburg (Germany).

The experiments were conducted in an office-like room under day-lit and artificially lit conditions where the participants were asked to perform a sequence of standardised office tasks (total of 125 participants, of which 28 participated in pilot studies (Sarey Khanie et al. 2011, 2013, 2013) and 97 in a main study, We considered five different daylight conditions and one artificial lighting condition.

The test facilities consisted of a set of two rooms located on top of the four-storey ISE main office building (latitude 48.00° N, longitude 7.83° E) that can be fully rotated. The flexibility allowed by the rotation was crucial to adjust the orientation of the test facility to a pre-defined sun azimuth angle so as to keep daylighting conditions under experimental control over the duration of the experiments. The range of this orientation was limited to Southwest and West. The two orientations were tested in a previous study (Sarey khanie et al. 2013) and showed no significant effect on gaze behaviour. The rooms are of typical single office size (3.5m wide x 3m high x 4.5m deep) with the following photometric properties: ρ_{wal}l = 0.62, $\rho_{ceiling}$ = 0.88,

ρ_{floor} = 0.11, and include one glazed façade (colour-neutral, double glazing: U-value = 1.1 W/m2K, g-value = 0.29). The distance between the desk and the window and the wall behind it were set to architectural standard for single office rooms (Neufert 2012).
The computer screen used for the experiments was a Samsung LED screen with a 19" screen size. The tilt angle of the computer screen was set to 10° from vertical. The distance between the centre of the screen plane to the edge of the desk was set to 550 mm to allow for readability of the characters on the screen (Herrmann & Scheuer 2004, ISO/9241-12 1998). The office chair used in the experiment was a padded, wheeled chair of adjustable seat height with no armrest. Fig. 1 shows the layout of the test rooms, the position of the participant in different parts of the test procedure, the measurement devices and their positions and all other objects used during the experimental trial or present in the scene.

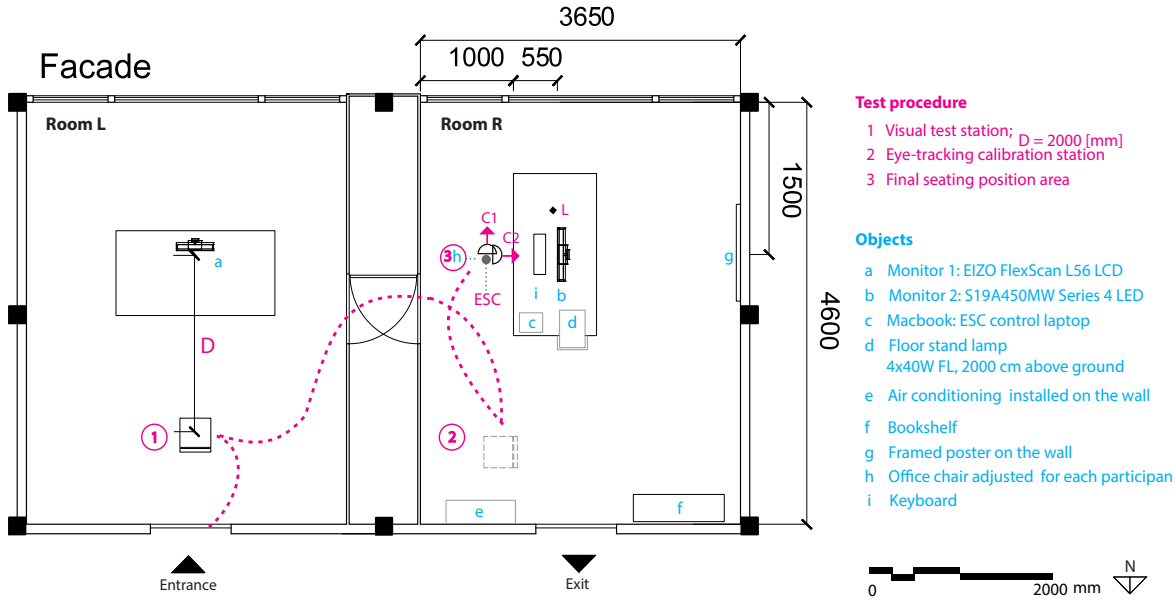

Figure 1 – The figure shows: the layout of the test-rooms

2.2 Photometric and gaze monitoring

The office-like room was equipped with measuring instruments. The photometric data was recorded with two calibrated CCD cameras equipped with fish eye lenses using high dynamic range imaging techniques. The luminance measurement was using a pair of calibrated CCD cameras (LMK 98 Luminance Video Photometer, LMK 98-4 colour, both with a Nikon FCE8 lens, FOV 183°). The cameras were mounted on a simple structure so as to be positioned above the participants' head with 90° rotation from each other Fig. 2b.
Eye and head movements were registered continuously using a state-of-the-art wearable mobile eye tracker (EyeSeeCam, www.eyeseecam.com) Fig. 2(a). We used large FOV luminance map HDR imaging techniques for characterisation of the luminous environment for a 270° span Fig. 2(b). The EyeSeeCam is a state-of-the-art lightweight head mounted eye tracker (Schneider 2009) equipped with three cameras. This eye-tracker measures both eyes pupil positions with two IR-sensitive cameras (Fig. 2a, camera 2 & 3), i.e. video-oculography (VOG). The EyeSeeCam software transforms these pupil detection data in real-time into head-referenced eye positions, which is referred to as eye-in-head coordinates in this paper. Additionally, an integrated inertia measurement unit (IMU) records head movements, i.e. rotation velocities and translative accelerations. A camera located on the forehead records point of view (POV) videos to an AVI format (Figure 2a, camera 3). All data streams are synchronised, so they are with the POV video, such that their information are mutually combinable. The mobile EyeSeeCam minimally limits the participant's movements and allows for natural exploration of the scene. In essence, we processed the following raw data:

- Eye-in-head positions from VOG at a frame rate of 221 Hz.
- A scene video recorded with a wide angle POV camera that is configured to a resolution of 366x216 pixels at a sampling rate of 25Hz.

- Angle velocities and translative accelerations from the IMU deliver relative head rotations and up to a certain limit relative head translations, both at synchronised 221Hz.

Knowing the 3-dimensional (3D) properties of the test room geometry and the experimental set up including the position of the cameras and the participants' initial head position Fig. 2(c), the gathered eye-tracking data (eye-in-head and head-in-world movements) can be transferred into world coordinates for computing the actual gaze-in- world directions.

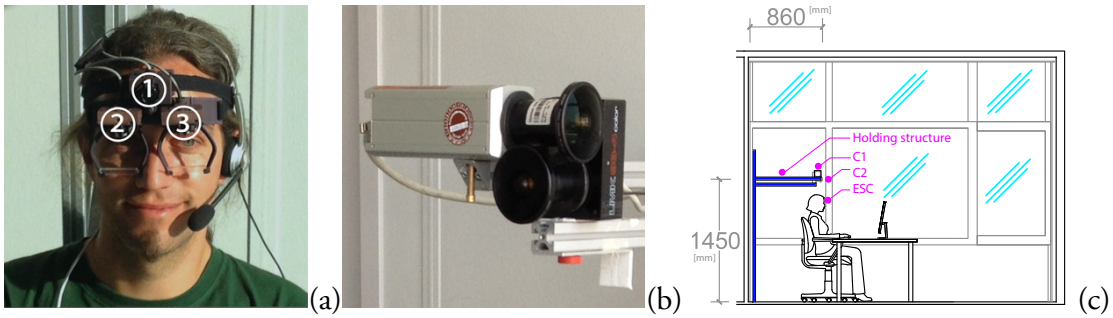

Figure 2 – (a) EyeSeeCam is equipped with three cameras, 1. Head-fixed scene camera, 2. & 3, (b) the two CCD cameras are installed above the participants head position, (c) the section showing the position of the CCD cameras and the approximate position of the EyeSeeCam mounted on the participants head.

Table 1 –lighting conditions

Each participant has evaluated one condition
LC1: Clear sky, no sun inside,
LC2: Clear sky, sun on the wall
LC3: Clear sky, sun on the desk,
LC4: Clear sky, sun in the FOV,
LC5: Overcast sky, no system,
LC6: Artificial light, window covered
Total number of subject: 97

Table 2 – photometric conditions

LC	$\bar{E}_v$ [lux]	L_m [cd/m^2]	L_s [cd/m^2]	$\bar{\omega}_s$ [sr]	$\#\bar{L}_s$
1	1200	300	4538	0.43	1.5
2	1800	600	2903	0.35	2.5
3	3000	1000	3919	0.33	4
4	5800	2500	45039	0.07	9
5	1000	400	2191	0.27	2
6	300	1000	1064	0.08	1

L_m is the average luminance of each image.

2.3 Task design and sequence

the order of utilisation of the task-supports was randomised for each participant). Using each task-support, the participants performed an office task sequence specifically designed for these experiments. Each office-task sequence consisted of four main phases: 1) *Input* phase, 2) *Thinking* phase, 3) *Response* phase and 4) *Interaction* phase.

63 males and 34 females, in the age group of 20 to 60 were recruited from the Fraunhofer ISE staff to participate in the experiment. The relevant body at Fraunhofer ISE approved the procedure and each participant volunteered to participation and gave informed consent. All participants were German speakers to avoid any bias due to lack of comprehension of the read and written tasks. On a continuous scale from "not at all sensitive" to "very much sensitive", 65\% of the participants considered themselves sensitive to brightness (rating > 1/2 of the scale line).
The participants were randomly assigned to the lighting conditions. Four of the lighting conditions were achieved under clear sky, one under overcast sky and in the last condition the window is completely blocked and an electrical floor stand fixture is present in the scene. The specification of each lighting condition is shown in table 1 & 2. The between group effects are six lighting conditions and the within group effects are two task-supports (computer screen and phone).
The test procedure started with the participants entering from the outside, first through the neighbouring room (Room L), and then to the test scene (Room R) so as to have similar adaptation to the indoor's environment. After entering the test scene, the eye-tracker was

calibrated for each participant in this room (Room R). The calibration procedure takes about 10 to 15 minutes, which allows for the participants to have proper visual adaptation to the lighting condition of the room. A socio-demographic questionnaire (on paper) was filled as well as the first lighting condition assessment questionnaire before starting the task activities.

3 Generation of gaze-centred luminance image

As the first step towards a gaze-driven luminance image, the dominant gaze directions were identified. The gaze directions where then translated to the luminance camera coordinate system after camera position corrections and considering misalignments, e.g. through slipping of the eye-tracker on the participant's head. A tool was developed to extract the luminance pixels from two captured luminance HDR images corresponding to 180° of the FOV with respect to the direction of the actual gaze. As a result, for each individual dominant gaze direction a new luminance image was produced showing the luminance distribution in the FOV experienced by the participant. In summary the following steps were made to derive luminance-fields relative to each dominant gaze direction Fig. 3.

- STEP I: Gaze-in-world orientations were measured
- STEP II: Dominant gaze directions were identified
- STEP III: Gaze-centred luminance images were derived

The gaze-driven luminance images were then compared with two fixed-gaze orientation assumptions: task orientation and 45° orientation.

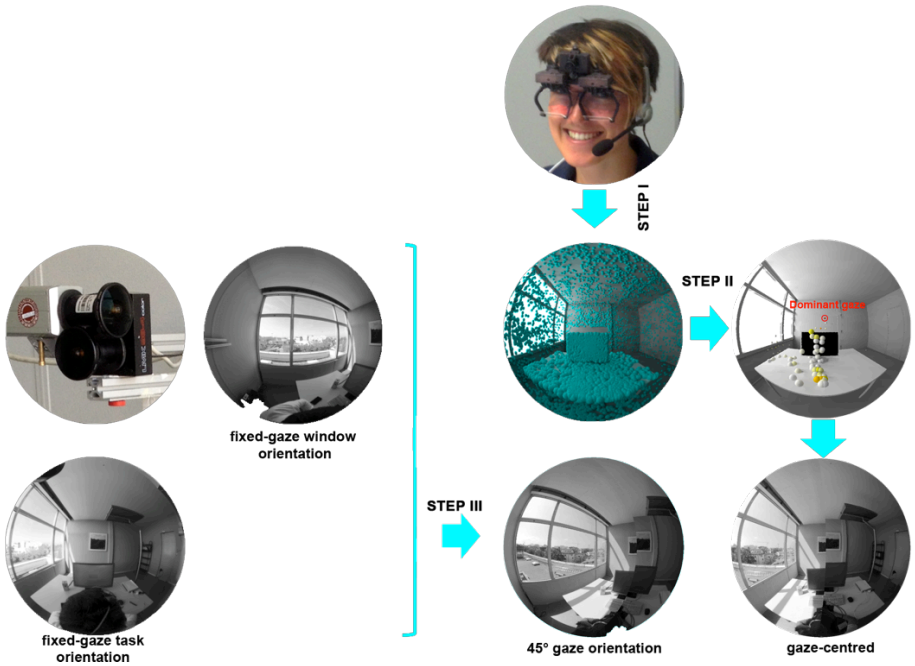

Figure 3 – the gaze-centred luminance images were produced in 3 steps.

3.1 Step 1: Gaze-in-world orientations

Based on the data generated during the experiments, a conversion to room referenced coordinates for head and gaze is realized. The eye-in-head data, which is a head, referenced eye coordinate, is obtained directly from the device using its intrinsic calibration. The recorded eye-in-head data rely on a prior calibration with a 5-point laser diffraction pattern that was performed successfully for each participant.
The gaze-in-world coordinates were first computed from the scene-camera 2D video records and then interpolated at high temporal resolution using the IMU acceleration data. The IMU acceleration data were applied to interpolate between absolute head orientations and positions, that we extracted approximately every 2nd second by 3D pose estimation from the scene camera.

In order to map coordinates from the scene-camera image to room-fixed coordinates, we defined 12 locations in room-fixed coordinates that are known from the computer aided design (CAD) model of the set-up, covered well within the 270° field of the LMK cameras not too eccentric in the scene: the four corners of the screen, the corners of the window, corners of the desk and corners of the door shown in Fig.4. For each analysed frame, we manually selected the 4 key points most central to scene-camera image.

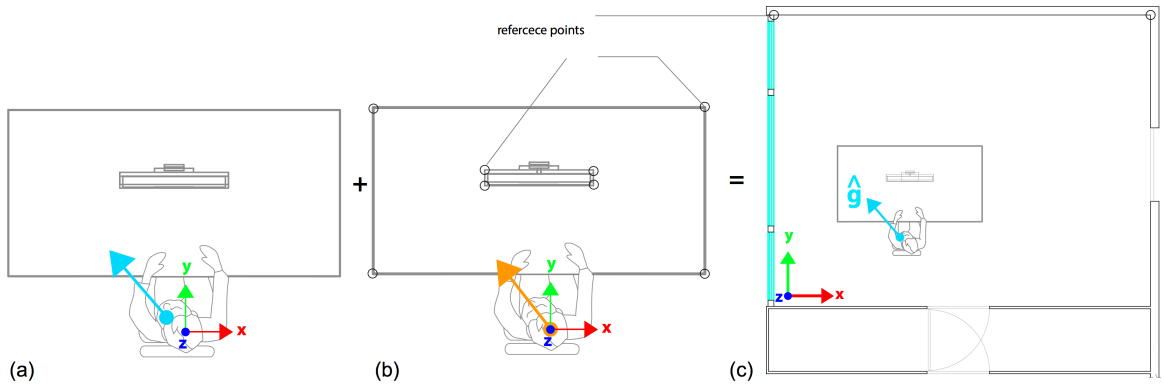

Figure 4- the gaze-in-world coordinates are derived from: (a) the eye-in-head coordinates superimposition with the (b) head-in-room coordinates to derive (c) the gaze-in-world coordinates.

The key-frame selection was done every 30s (750 frames) or in case of a gaze shift (resulting in a new scene frame). This procedure ensured that we obtain head-coordinates had a high resolution to be synchronized to the IMU sensors, and later on matched to the eye-tracker's sampling rate. Additionally, in this procedure the head tilts were detected and a rotation matrix was derived to rotate the eye-in-head eye-in-head direction around y-axis by the negative tilt angle β Fig 5(b).

The resulting head-in-room coordinates were aligned with the setup such that a head orientation straight ahead when sitting at the desk (POV camera's optical axis) was parallel to the y room reference axis. Fig. 5(a) shows the coordinate system with the origin (0,0,0) at the head position. Gaze orientations are rotated analogously to Euler angles with the polar angle φ between -180° and 180° for head rotations around the vertical room axis, the azimuth angle Θ between -90° and 90° for down and upward directing, Fig. 5(a), and the angle β for sideward head tilts. Thus, for example while setting each other angle to zero, α maps rotations around the z room reference axis, γ around the x axis and β around the y axis Fig. 5(b). The eye-in-head angles have the same rotation axes as the resulting head-in-room angles φ and Θ and are superposed together using several features of a camera calibration tool (Bouguet 2004) in order to obtain gaze-in-world vectors $\hat{\mathbf{g}}$ Fig 4(a-c).

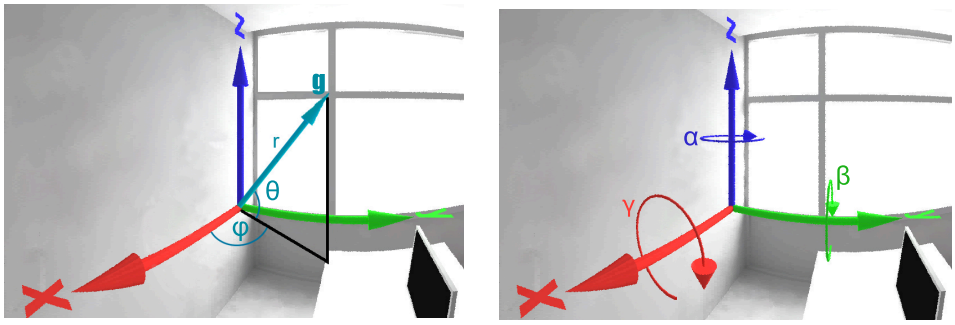

Figure 5- EyeSeeCam coordinate system: (a) EyeSeeCam coordinate system in the room, (b) spherical coordinates of the gaze vectors in the 3D space. The Euler rotations are shown with the angular rotations of β, γ and α.

3.2 Step 2: identifying the dominant gaze directions

The spatial distribution of the fixation points were measured based on a *spatial dispersion* method (Salvucci et al. 2000). This method focuses on the probability density of the fixation points over the visual space. The angular positions of the highest frequency of gaze encounter were then considered as the dominant gaze directions Fig. 6(a). The gaze directions were binned with a 5° width, which encompasses foveal (up to 1.5°) and para-foveal components (1.5° up to 5°) of the central vision Fig.6 (b, c). In this method we minimised the risk of selecting a pre-assumed gaze position present in other methods, e.g. averaging, clustering, weighted averaging etc.

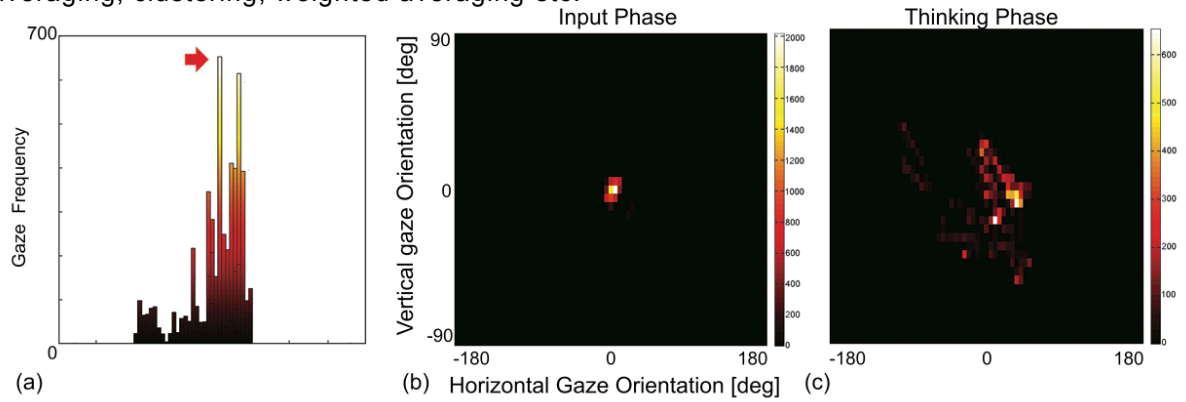

Figure 6- gaze distribution: (a) a histogram of gaze distribution; the x-axis corresponds to 180° horizontal gaze orientation; the y-axis and colour bar shows the number of gaze encounters at each point in space (highest for the dominant gaze direction , shown with arrow). b, c) One participant's gaze binned for on-screen *Input* phase and *Thinking* phase; the y-axis corresponds to vertical gaze orientation.

Figure 7(a-d) demonstrates one participant's gaze allocations during each task phase using screen as task-support. The darker points show the higher fixation frequency. The size of spheres in each image represents the number of gaze encounters on that point. As the data is represented in 3D space, the further the spheres fall, the smaller they look. To avoid this effect we rescaled the spheres based on the distance of the allocation point to the viewpoint.

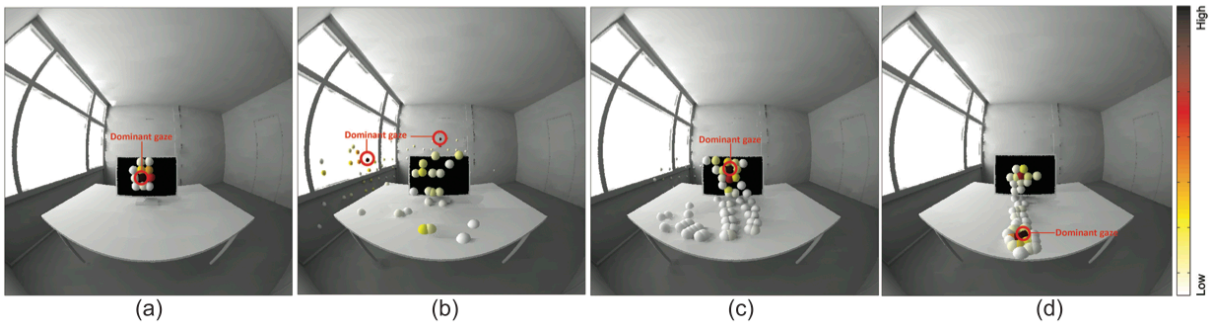

Figure 7- 3D visualisation of the gaze allocations in each task phase: (a)*Input* phase, (b) *Thinking* phase, (c) *Response* phase, (d) *Interaction* phase.

3.3 Step III: Deriving gaze-centred luminance images

The dominant gaze directions were used to derive the adaptation luminance in the FOV by generating gaze-centred luminance images. In order to translate the gaze direction vectors to the luminance images, we used lighting simulation tool *Radiance* (Ward-Larson 1998) and the CAD 3D geometrical model of the test room. Having the actual gaze direction vector properties in the luminance camera coordinate system (origin: camera position), we were able to extract luminance images corresponding to each vector from the two captured images. For this a new tool was developed which took the luminance images and the vector coordinates as input and generated one luminance image with respect to the input vector as the centre of the image.

4 Results

For each experimental trial consisting of 8 phases, fixed-gaze task (screen) orientation, gaze-centred and 45° gaze orientation luminance images were generated and processed using an evaluation tool *Evalglare* (Wienold & Christoffersen 2006) for deriving the adaptation levels in terms of Illuminance at the eye level (E_v).

Figure 8 demonstrates the derived E_v for the two approaches. The x-axis represents the gaze-driven E_v and the y-axis he fixed gaze E_v. Comparing the task phases we can see that the On-screen Input phase is less affected by the gaze-driven measurement. The rest of the task phases show more sensitivity towards the gaze orientations. These task phases leave room for observing task independent gaze behaviour in relation to different adaptation levels. Figure 9 (a, b) compares the gaze-driven approach to a task oriented gaze and 45° gaze orientation towards the window.

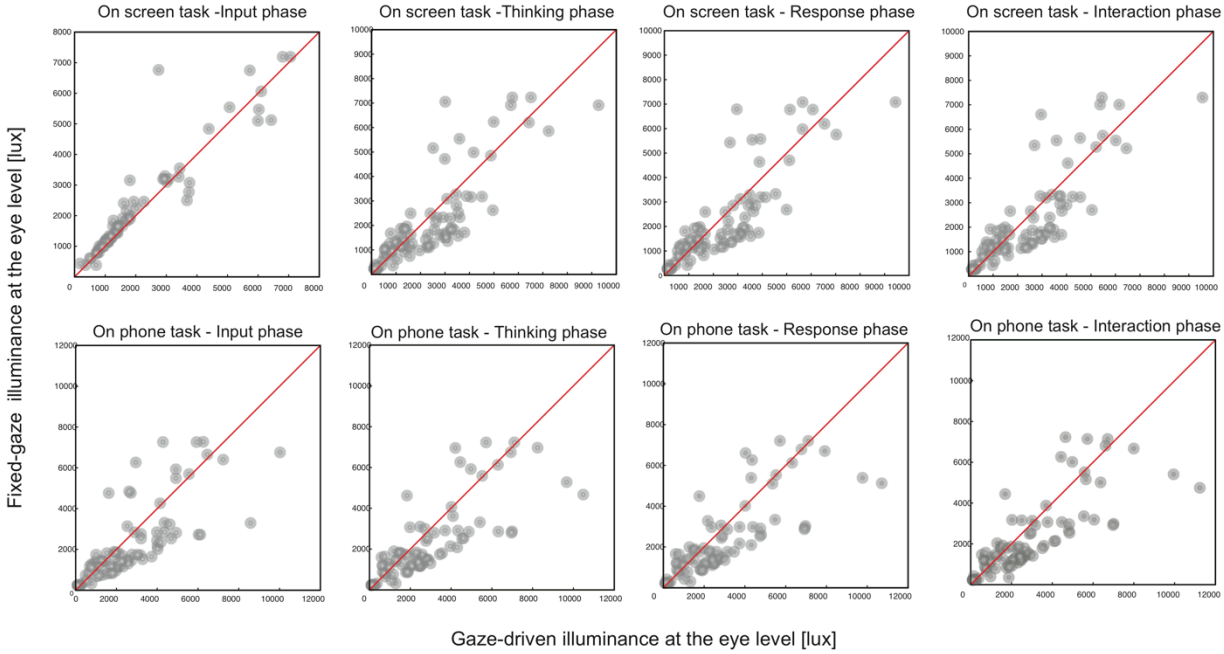

Figure 8 - Illuminance at the vertical level for gaze-driven vs. fixed-gaze approach for the 8 task phases using two different task-supports.

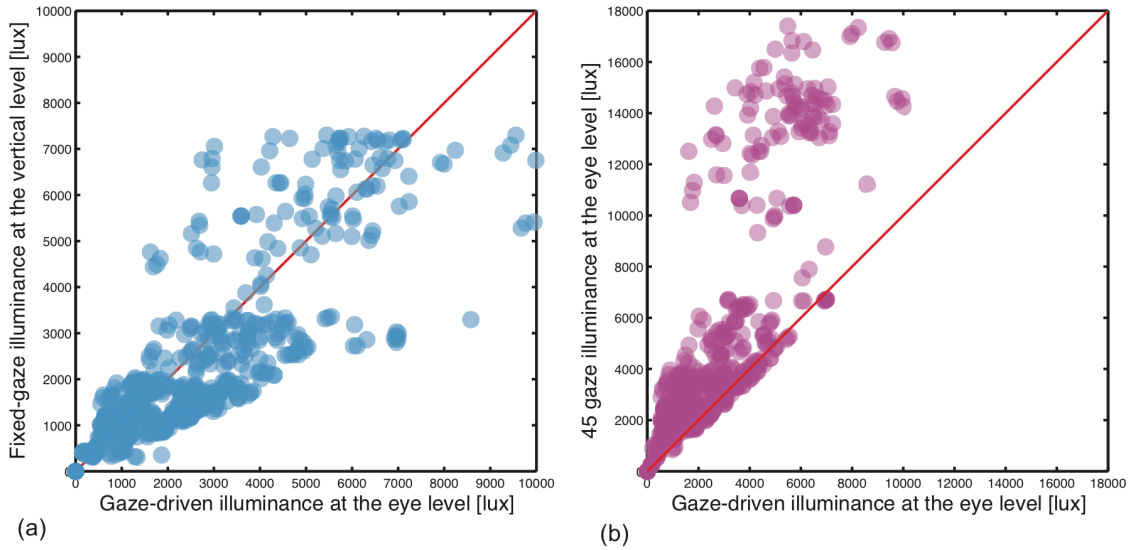

Figure 9: Illuminance at the vertical level: (a) Gaze-driven and fixed-gaze task orientation. (b) Gaze-driven and 45° gaze orientation towards the window.

Exploring the data we can see that the gaze-driven and fixed-gaze approaches behave differently as the illuminance at the vertical level rises Figure 9(a). Here, we can observe prominent gaze behaviour: as the E_v values increase, there is a shift of gaze-driven E_v to the lower values. This effect is opposite for lower vertical illuminance levels where the gaze is oriented towards the higher luminance levels. Between 3000 and 4500 lux the number of data points are low due to the experimental set up constraint. Comparing the gaze-driven approach to the 45° gaze towards the window, we can see that a window orientation results in higher values than the actual gaze orientation.

To quantify the difference between the two approaches, A one-way ANOVA test was performed on the illuminance at the vertical level derived from the three gaze approaches (table 3): gaze-drive, 45° gaze and the fixed gaze assumption. The difference between the three approaches are significant ($F(2, 1965)=140$, *P-value*<0.0001). The boxplots show distribution of the illuminance at the vertical level for the three approaches. The difference between the gaze-driven and the 45° gaze orientation ($F(1, 1310)=138.52$, *P-value*<0.0001) is greater than the differences between the gaze-driven and fixed-gaze task orientation ($F(1, 1310)=9.96$, *P-value*<0.01).

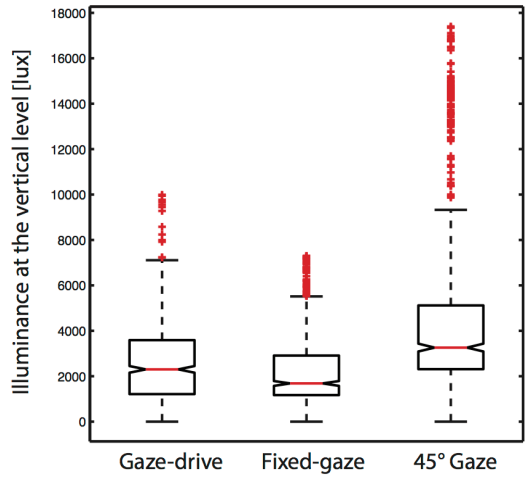

Table-3 one-way ANOVA results

Source Gaze-driven = a Fixed-gaze = b 45° Gaze = c	a x b	a x c	a x b x c
F	9.96	138.52	140
P-value	0.0016	1.8×10^{-30}	6.1×10^{-58}
SS	3.4×10^{7}	1.4×10^{9}	2.2×10^{9}
MS	4.5×10^{9}	1.4×10^{9}	1.5×10^{10}
df	1	1	2
Error	1310	1310	1965

Figure 10: A boxplot showing the illuminance at the vertical level distribution for the three approaches

5 Discussion and main findings

The results demonstrate that visual office task is a main drive for gaze orientations. When working with a computer, the gaze is mainly attracted to the task-area. The fixed-gaze task-assumption, hence, is an accurate gaze orientation assumption for measuring the luminance variations in the FOV. This assumption is adopted by the existing glare metrics. However, selecting a task position precedes the gaze point and direction assumption.
Primarily, this result highlights the importance of the task position in workplace design. A gaze responsive task positioning, can enhance the visual comfort qualities in a wok place.

A comparison between the gaze-driven approach and fixe-gaze approach oriented toward the task shows that the gaze is oriented towards higher values when the adaptation levels are low. This behaviour is opposite when the adaptation levels increase. A window orientation which was measured with a 45° gaze orientation towards window results in much higher values to what is selected preferentially by gaze. Therefore, a fixed-gaze assumption with orientation towards window is not a good measure for luminance estimation in FOV.

The prominent outcome of the study was that the gaze behaves differently for different adaptation levels. It is thus important to observe the gaze behaviour in relation to light to have a better understanding of the natural gaze behaviour towards different lighting conditions.
In future steps, gaze behaviour in relation to light and view, which are the two main components of a window, are going to be analysed.

6 Conclusion

In this paper the integration procedure of the luminance images coupled with eye tracking for obtaining the gaze-driven luminance fields is described in detail. The gaze-driven luminance fields were derived in three major steps. The first step was to compute the gaze directions in the real scene (gaze-in-world) from the data recorded by the eye-tracker. The second step was to identify the gaze directions that were dominant (i.e. most frequently used) during each phase of the experiment, hence determining dominant field(s) of view for each task and participant. The final step was to derive the luminance distribution within the FOV with respect to the resulting dominant gaze direction(s). We then compared gaze-driven luminance field measurements to fixed gaze luminance field measurements. The resulting images were processed using *Evalglare.* This tool is one of the available Radiance based tools for processing HDR images for glare risk evaluations. The main output of the tool used in this study is illuminance at the eye level.

The results show that there is a significant difference between gaze-driven luminance approach and fixed-gaze assumption approach. The gaze-driven approach was compared to the fixed-gaze approach directed towards the task and fixed-gaze approach directed 45° towards the window. This difference was larger for higher luminance levels within the field as our exploratory data analysis shows that the gaze avoids regions with higher luminance levels We also observe that the visual task overrides light-induced gaze shifts. Importantly, the differences between the gaze and fixed-gaze approach demonstrate that the gaze behaves differently in different luminance adaptation levels. This major finding demonstrates the importance of gaze behaviour for accurate glare evaluation. Moreover, the findings suggest that the assumption of gaze fixation on the task area is an accurate assumption. This, however, highlights the importance of selecting a given gaze-driven task-area position. The gaze detection is a pre-requisite for accurate glare evaluation. A gaze-driven visual comfort assessment, hence, is needed in order to detect the gaze-dominant regions of space.

In future studies, the two approaches will be evaluated against subjective assessments of glare discomfort glare. This evaluation will demonstrate whether a gaze-driven luminance estimation in relation to the subjective assessments give a better prediction for risk of discomfort glare situations than using the fixed view assumption. Moreover, the gaze behaviour in relation to different lighting conditions will be studied to further our understanding of the dependencies of visual discomfort and gaze patterns.

7 Acknowledgment

The Ecole Polythechnique Fédérale de Lausanne (EPFL) and German Research Foundation (SFB/TRR 135 and EI 852/3 to WE) supported this project. The authors wish to thank C. Reetz at PSE Freiburg for his technical contribution. We are grateful for the granted access to Fraunhofer ISE test facilities and thank the ISE staff and non-ISE participants that took part in the experimental study.

References

Bouguet, JY. (2004), *Camera calibration toolbox for matlab*.

Boyce, PR. (2014), *Human Factors in Lighting*, Third Edition. CRC Press.

Clear, R. (2012), *Discomfort glare: What do we actually know?,* Light Res Technol.

Herrmann, HJ. Scheuer, S. (2004), *Requirements for new technologies becoming part of on-screen works as well as directions for their implementation, especially in standardization activities.* Report F 1846. Federal Institute for Occupational Safety and Health.

Hopkinson, R.G. (1972), *Glare from daylighting in buildings*. 3(4):206–215.

Hubalek, S., Schierz, C. (2004), *LichtBlick–photometrical situation and eye movements at VDU work places.* In: CIE Symposium. 322–324

International Commission On Illumination (CIE). (1983), *Discomfort glare in the interior working environment*.

ISO/9241-12. (1998), *Ergonomic requirements for office work with visual display terminals (VDTs), Part 12: Presentation of information. International Standard.*

Jakubiec, J.A., Reinhart, C. F. (2012), *The 'adaptive zone'–a concept for assessing discomfort glare throughout daylit spaces.* Light Res Technol. 44(2), 149–170.

Kim, W. Han, H., Kim, JT. (2009), *The position index of a glare source at the borderline between comfort and discomfort (BCD) in the whole visual field*. Building and Environment, 44(5),1017–1023.

Kokoschka, S. Haubner, P. (1985), *Luminance ratios at visual display workstations and visual performance*. Light Res Technol. 17(3), 138–144.

Luckiesh, M. Guth, S.K. (1949), *Brightness in visual field at borderline between comfort and discomfort (BCD).* Illuminating engineering.

Neufert, E., Neufert, P. (2012), *Architects' data*. John Wiley & Sons.

Nuthmann, A., & Einhäuser, W. (2015) *A new approach to modeling the influence of image features on fixation selection in scenes. Annals of the New York Academy of Sciences.* 1339:82-96.

Salvucci, DD., Goldberg, JH. (2000), *Identifying fixations and saccades in eye-tracking protocols. In: Proceedings of the 2000 symposium on Eye tracking research & applications*. ACM, 71-78.

Sarey Khanie, M., 't Hart, M., Stoll J., Einhäuser W., Andersen M. (2011), *Integration of Eye-tracking Methods in Visual Comfort Assessments.* CISBAT 11: CleanTech for Sustainable Buildings - From Nano to Urban Scale, Lausanne, Switzerland.

Sarey Khanie, M., Stoll J., Mende S., Wienold J., Einhäuser, W., Andersen M. (2013), *Investigation of gaze patterns in daylit workplaces: using eye-tracking methods to objectify view direction as a function of lighting conditions.* In: Proceedings of CIE Centenary Conference" Towards a New Century of Light." CIE Central Bureau, 250–259.

Sarey Khanie, M., Stoll J., Mende S., Wienold J., Einhäuser W., Andersen M. (2013), *Uncovering relationships between view direction patterns and glare perception in a daylit workspace.* In: LUXEUROPA.

Schneider, E., Villgrattner, T., Vockeroth, J., Bartl, K., Kohlbecher, S., Bardins, S., et al. (2009), EyeSeeCam: An Eye Movement-Driven Head Camera for the Examination of Natural Visual Exploration. *Ann N Y Acad Sci.* 1164(1),461–467.

Sury, P.M., Hubalek, S., Schierz, C. (2010), *A first step on eye movements in office settings*: Eine explorative Studie zu Augenbewegungen im Büroalltag, volume 51. GRIN Verlag,.

Vincent, BT., Baddeley, R., Correani, A., Troscianko, T., Leonards, U. (2009), *Do we look at lights? Using mixture modelling to distinguish between low-and high-level factors in natural image viewing. Vis Cogn.* 17(6-7), 856–879.

Ward-Larson, G. Shakespeare R. (1998), *Rendering with radiance: the art and science of lighting visualization*. San Francisco, CA, USA: Morgan Kaufmann Publishers Inc.

Wienold, J., Christoffersen J. (2006), *Evaluation methods and development of a new glare prediction model for daylight environments with the use of CCD cameras*. Energy and Buildings 38(7), 743–757.